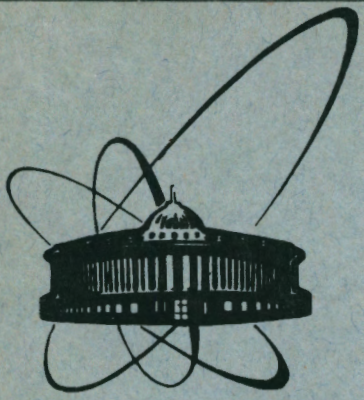

сообщения
объединенного
института
ядерных
исследований
дубна

E13-91-175

L.M.Soroko

INVERSE MESO-OPTICS AND ITS POTENTIAL APPLICATIONS

1991

1. INTRODUCTION

The term "meso-optics" was introduced in[1] to cover a wide class of nontraditional optical devices, which accomplish the homomorphic (nonreversible) transformations of the object space under which the dimension of the image is getting greater than the dimension of the object in the frame of the geometro-optical approximations. For example, an axicon or a conical lens transforms the point on the optical axis into the straight line segment. The focal line length of the axicon is defined only by the geometrical factors and does not depend on the diffraction of the light. Another example of the meso-optical elements is the meso-optical mirror with ring response[2] or its kinoform equivalent[3]. In the meso-optical Fourier transform microscope[4] the point is transformed into a short shirt. This is an example of the zero-dimension (0D) → two-dimension (2D) homomorphic transformations.

Unlike the classical optical imaging devices in which the divergent spherical wavefront is transformed into a convergent spherical one, in meso-optics we deal with conical wave-fronts. For example, an axicon transforms a divergent spherical wavefront into a convergent conical wavefront which collapses on the optical axis into the long zero-order diffraction order surrounded by the circular side lodes. Untill recently meso-optical elements were used only for metrological purposes[5,6]. The meso-optical Fourier transform microscope[4] was the first meso-optical device which has been used as an imaging element for straight line particle tracks in the three-dimensional volume. The meso-optical confocal microscope[7] offers very long depth of focus and has weak circular side lobes in the output image.

The longitudinal interference of the conical wavefronts sometimes named as "diffraction free wavefronts" was investigated in the papers[8,9,10]. The experimental unit for observation of such phenomenon and a technique for suppression of the longitudinal modulation of the light intensity are presented in[8]. The experiments on longitudinal interference of the conical wavefronts produced by the screen with narrow coaxial transmitting rings are described in[9]. The possible applica-

tions of the longitudinal interference of the conical wavefronts are given in[10]. There was suggested the confocal meso-optical keratometer for fast remote measurement of the object profile without any computer reconstruction inherent to the traditional optical keratometer and with high depth of focus. The confocal meso-optical profilometer generating the chirp-modulated longitudinal interference pattern was proposed in[10] as well. In such a device we have no abiguities arisen in the case of the object profile with sharp kinks.

The properties of the inverse meso-optics and its potential applications are described in this paper. The definition of the inverse meso-optics is given. The necessary conditions under which the inverse meso-optical transformation can be accomplished are treated in the frame of the phenomenological model. A very long straight line regment must be transformed into the point in the image space. Two examples of the applications of the inverse meso-optics will be treated: differential Čerenkov gas counter with high radiation density and with small residual chromatic effects and meso-optical elements for synchrotron radiation from undulator which goes side-wise to its optical axis. The optical properties of the self-focusing undulator are given.

2. MESO-OPTICS

To illustrate the properties of the conical wavefronts let us consider two pictures. In Fig.1 we see the production of the cylindrical wavefront which can be treated as an envelope of many spherical waves of the wave length λ issued coherently with the common phase from all points of the straight line segment AB. We neglect the radiation which goes along the Z-axis. If the spherical waves are radiated with phases that are changing linearly along the straight line segment CD (Fig.2), we get the conical wavefront with the same axis of symmetry. The latter example slows that the conical wavefront can be considered as an array of many spherical wavefronts issued coherently from the points of the straight line segment.

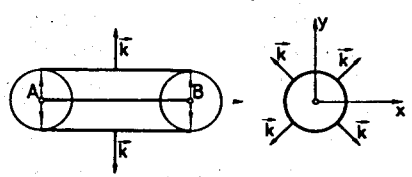

Fig.1. Production of the cylindrical wavefront as an envelope of many spherical waves of the wavelength λ which issue synchronously from the point of the straight line segment AB.

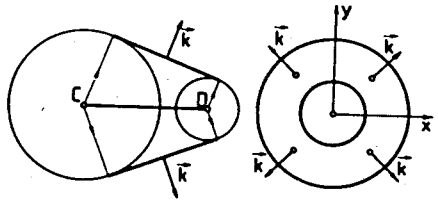

Fig.2. Production of the conical wavefront as an envelope of many spherical waves of the wave length λ which issue with phase delay changing linearly along z-axis from point to point of the straight line segment CD.

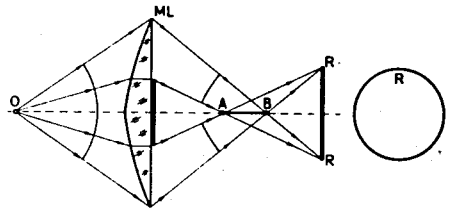

Fig.3. The meso-optical element ML which transforms the point on the optical axis 0 into the straight line segment AB and into the ring R in different parts of the image space.

Let us consider the meso-optical element which transforms the divergent spherical wave into the wavefield which contains not only spherical convergent waves but the conical ones as well (Fig.3). This meso-optical element is a rotation figure with generating line having kink on the optical axis. Owing to this configuration the point on the optical axis is transformed into the brilliant straight line segment AB and brilliant focal ring R which are in different parts of the image space.

The coherently, in phase, radiated points of the ring-shaped radiator (Fig.4) produce quasiconical wavefront in which the wavevectors $\vec{k}$ in the meridional cross section are not directed identically in different parts of the space. In this case the brilliant segment extends from $-\infty$ to $+\infty$ along z-axis.

In the case of two concentric ring-shaped radiators we observe the longitudinal interference of two quasiconical wave-

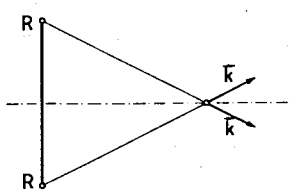

Fig.4. The wavefield produced by the ring-shaped radiator R with all points in phase for the wavelength λ. The meridional cross section of the system is shown.

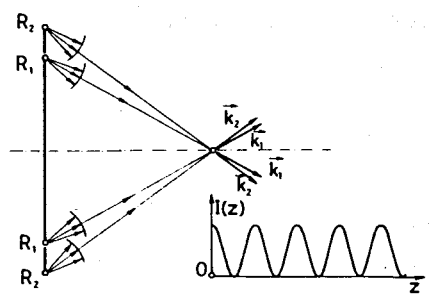

Fig.5. The longitudinal interference of two quasiconical wavefronts produced by two concentric ring-shaped radiators R_1 and R_2: top - the meridional cross section of the system, bottom - the modulation of the light intensity on the optical axis of the system.

fronts. The light intensity on the optical axis is modulated along z-axis[10] (Fig.5).

The meso-optical element with ring response is of great value as this element has been used as an imaging element in the meso-optical Fourier transform microscope[1,2,19]. In some cases instead of meso-optical element with ring response the cylindrical lenses can be used[7,9,23].

3. CONICAL WAVEFRONT

The analytical representation of the conical wavefront is given in[11]. The time-independent scalar homogeneous wave equation was solved for homogeneous medium with generator in the form of a luminuous line of infinite length. The solution was given in the cylindrical coordinates ρ, z, ϕ. To present this solution in a pictural form let us consider the meridional cross section of the space with z-axis as a symmetry axis (Fig.6). The wave vector $\vec{k}$ of the conical wavefront at large distances from z-axis has a constant value with two components:

$$k_z = k\cos\theta,\quad k_\rho = k\sin\theta, \tag{1}$$

where θ is the wadge angle of the conical wavefront or the angle between the wave vector $\vec{k}$ and the z-axis.

The wave function of the conical wavefront has the form:

$$u(\rho,z,t) = \frac{\exp(-i\frac{\pi}{4})}{\pi\sqrt{k_\rho\rho/2\pi}}\exp(-i\omega t)\cdot\exp[i(k_\rho\rho + k_z z)], \tag{2}$$

where ω - the angular frequency of the radiation of the wavelength λ, and $tg\theta = k_\rho/k_z$.

In the region of the collapsed line on the z-axis the convergent conical wavefront produces the circular diffraction pattern with radial light intensity distribution:

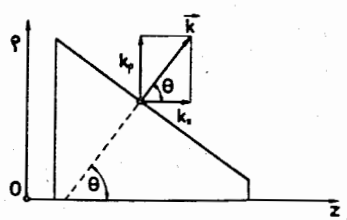

$$I(\rho) = \text{Const}\cdot J_0^2(k_\rho\rho), \tag{3}$$

Fig.6. The meridional cross section of the conical wavefront in the form of the semiplane with $\rho \geq 0$ and wave vector $\vec{k}$ (k_ρ, k_z).

where $J_0(\cdot)$ is the Bassel function of zero-order. For $\theta = 0$, $k_\rho = 0$, the conical wavefront goes into the plane wave

$$u(z,t) = \text{Const}\cdot\exp(ik_z z), \tag{4}$$

and for $\theta = 90°$ we have a cylindrical wavefront with $k_z = 0$ in (2).

4. INVERSE MESO-OPTICS

The first application of the inverse meso-optics was in the meso-optical confocal microscope[7,19] shown in Fig.7. The illuminating meso-optical objective 2 transforms the divergent wavefront from the point light source 1 into convergent conical wavefront which collapses into the straight line segment AB of the length L, convertes into the divergent conical wavefront and next goes to the imaging meso-optical objective 3. The latter transforms it into the convergent spherical wave. The point photodetector 4 accepts this spherical wave. The imaging meso-optical objective 3 is indeed an inverse mesooptical element as it transforms the divergent conical wavefront from the segment AB into the convergent spherical wave. In the meso-optical confocal microscope[7,19] the radiation from the straight line segment AB is a coherent one and owing to this we can realize the described sequence of transformations. The more complete explanation of the inverse meso-optics (IMO) is presented in Fig.8.

In another extreme case we have the noncoherent radiation from the segment AB with phases randomly distributed over this segment (Fig.9). Each point of the segment AB produces a divergent spherical wave which is transformed by the imaging meso-optical objective 3 (in Fig.7) into a segment on the optical axis. The point A goes into the segment A'A". The point B goes into the segment B'B". It is evident that the light intensity distribution on the optical axis can be approximated by the noncoherent sum of many brilliant segment which is a triangle

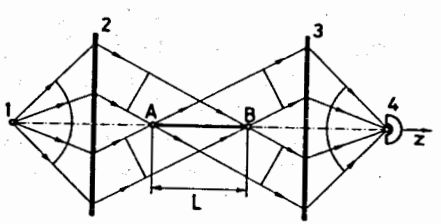

Fig.7. Confocal meso-optical microscope: 1 - point source, 2 - first meso-optical objective, 3 - second meso-optical objective, 4 - point photodetector.

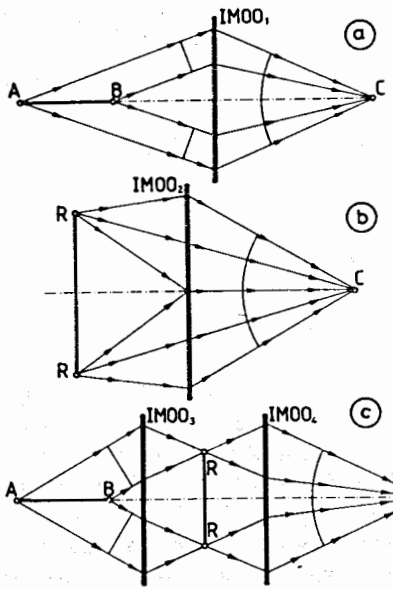

Fig.8. Principle of the inverse meso-optics (IMO): a) transformation of the conical wavefront coherently radiating segment AB into a point C by the inverse meso-optical objective $IMOO_1$; b) transformation of the coherent radiation from a ring-shaped radiator R into a point C by the inverse meso-optical objective $IMOO_2$; c) two-stage transformation of the coherent radiation from the straight line segment AB into the ring-shaped focus R at the first stage by the inverse meso-optical objective $IMOO_3$ and then into the point C at the second stage by the inverse meso-optical objective $IMOO_4$.

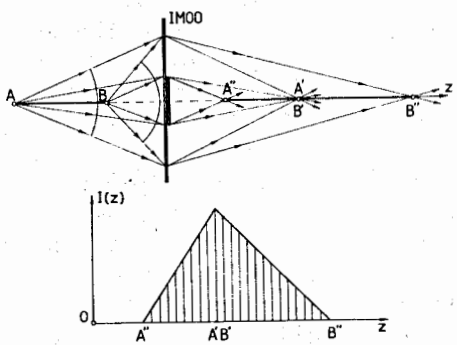

Fig.9. Transformation of the noncoherent radiation from a straight line segment AB by the inverse meso-optical objective IMOO into the triangle shaped distribution of the light intensity A″ B ″ on the optical axis (top). The light intensity distribution I(z) (bottom).

function with end points A″ and B″ and with maximum at the point A′ = B′.

From these examples we see that the necessary condition for sharp focusing of the radiation into one point focus F is the following one: the wavefront generated by the segment AB must be pure coherent for all points of the segment AB. However if this condition is not met, we can, nevertheless, put the pinhole before the photodetector in the point A′ = B′ (in Fig.9), thus to isolate the unique conical wavefront component which is present in the total noncoherent radiation from the segment AB. All other nonconical components will be suppressed. The analogous process of isolation is taking place in the case of the traditional lens. The pinhole placed in the focus F does isolate one spherical component which is collapsed into the focal point F. All other spherical waves will be rejected.

5. ČERENKOV COUNTER

The differential isochronic Čerenkov gas counter[12] consists of the gaseous radiator, spherical mirror 1, optical abberation corrector 2, optical chromatic corrector 3, the ring diaphram 4 and matrix photodetector 5. The Čerencov radiation of the charge particle is reflected from the spherical mirror 1 and concentrated into a ring (Fig.10). The ring-shaped diaphragm 4 transmits the Čerenkov radiation from particle with given velocity. The charge particles going parallel to the optical axis of the Čerenkov counter are defined by the electronic master system 6 and 7.

The angle of the Čerenkov radiation Θ of the wavelength λ is defined by the velocity v of the change particle and by the refraction index of the gas $n(\lambda)$:

$$\frac{\Theta^2}{2} = [n(\lambda) - 1] - (1 - \beta^2), \qquad (5)$$

where $\beta = v/c$, c - velocity of the light in the vacuum. The chromatic blurring of the Cerenkov radiation, induced by the severe dependence of $n(\lambda)$ from the wavelength λ, is the main problem of many Čerenkov counters.

The chromatic compensator in the counter[13] consists of the axicon and of the spherical lens. To correct the chromatic aberrations of the Čerenkov radiation and the coma aberration of the spherical mirror a double axicon lens of fused quartz and matrium chlorate crystal has been used[20]. In the Čerenkov counter[14] the correction of the chromatic aberration of the Čerenkov radiation is accomplished by the appropriate system of two lenses. To concentrate the Čerenkov radiation into a point a torric lens with generating line in the form of the circle arc was proposed in[26]. The torric lens is of course a meso-optical element but it does not suit to the conical wavefronts. The main shortcoming of the system[14] is that the blurring of the Čerenkov ring induced by the spherical aberra-

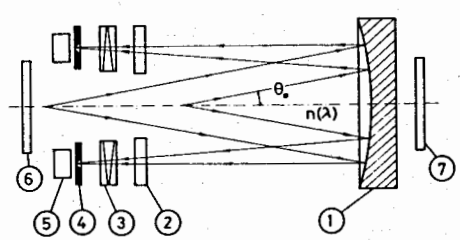

Fig.10. Traditional differential isochronous self-collimating Čerenkov counter: 1 - spherical mirror, 2 - coma corrector, 3 - chromatic corrector, 4 - ring-shaped diaphragm, 5 - photomultipliers, 6 and 7 - electronic master system.

tions and by the residual chromatic aberrations of the Čerenkov radiation is much bigger than the effects of the multiple scattering of the charge particles in the gas and by the diffraction of the light.

The origin of the spherical aberrations is that the source of the Čerenkov radiation in gas is not a single point but the straight line segment of the length ~2 m. The origin of the coma aberration is that the Čerenkov radiation consists of the conical wavefronts with the wavevectors of different orientations with optical axis of the Čerenkov counter. The chromatic aberrations of the Čerenkov radiation cannot be completely corrected as we have very restricted range of the optical materials for chromatic corrector consisting of two optical component with different behaviour of the refractive index $n(\lambda)$.

Some of these deadlock problems can be solved by means of the inverse meso-optics. In our system (Fig.11) there is the main mirror 1 with generating line as a segment of the parabola with axis oriented parallel to the wavevector of the Čerenkov radiation in the meridional cross section of the counter that is at the angle Θ_0 with optical axis of the counter, where

$$\Theta_0^2 = 2(n_0 - 1) - 1/\gamma_0^2, \qquad (6)$$

n_0 is the average refractive index of the gas, γ_0 is the average relativistic factor of the detected particle. The focal length of the parabola said is greater than the length of the radiator. The chromatic corrector 2 of the inverse meso-optical Čerenkov counter is a phase circular diffraction grating with the first diffraction order going to the optical axis of the Čerenkov counter. The backing of this circular diffraction grating is a conical surface with opening angle $(90^0 - \Theta_0)$. With this chromatic corrector we can suppress any linear λ-dependence in the refractive index $n(\lambda)$ of gas. The third element of our Čerenkov counter is a conical mirror 3 with internal reflected surface.

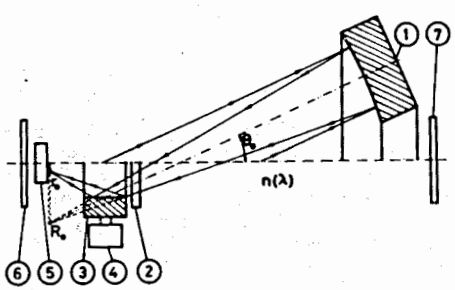

Fig.11. Meso-optical differential Čerenkov counter: 1 - meso-optical mirror, 2 - chromatic corrector, 3 - conical mirror, 4 - moving stage, 5 - matrix photodetector, 6 and 7 - electronic master system.

Let us consider the evolution of the light rays in this Čerenkov counter. The charge particle moving in gas with

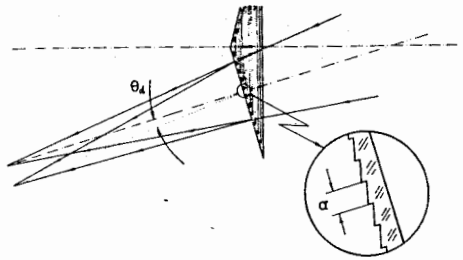

Fig.12. Meso-optical chromatic corrector in the form of the circular diffraction greating on the conical backing: Θ_d - diffraction angle.

average relativistic factor γ_0 produces the conical Čerenkov radiation. After reflection from the meso-optical mirror 1 the light rays are focused into a ring-shaped focus, one point of which in the meridional cross section is shown in Fig.11. The light rays cross at first the optical axis of the counter and only then produce the Čerenkov ring. Owing to this the coma aberration is absent for rays with $\Theta = \Theta_0$. The light rays are following on the chromatic corrector 2 perpendicular to its generating line. The properties of the chromatic corrector 2 (Fig.12) are defined by the diffraction grating equation

$$\sin \Theta_d = \lambda/a, \qquad (7)$$

with Θ_d - diffraction angle and with "a" - the pitch of the circular diffraction grating defined by the linear part of the function $n(\lambda)$ in the chosen spectral interval. The additional conical mirror 3 with internal reflection surface is designed to reduce the diameter of the Čerenkov ring or to focus all Čerenkov radiation into a point.

The relative chromatism of the circular diffraction grating is equal to

$$\frac{1}{f}\frac{\partial f}{\partial \lambda} = -\frac{1}{\lambda}, \qquad (8)$$

where f is the length of the light rays between circular diffraction grating and the photodetector 5 in Fig.11. The relative chromatism of the spherical refracting surface,

$$\frac{1}{f}\frac{\partial f}{\partial \lambda} = -\frac{1}{n(n-1)}\frac{\partial n}{\partial \lambda}, \qquad (9)$$

is about 20÷25 times smaller than for circular diffraction grating, Eq.(8). Owing to this the chromatic correction in our Čerenkov counter is attained at smaller diffraction angles than in the refractive chromatic corrector. All elements of the proposed Čerenkov counter can be fabricated as mirror ele-

ments. This opens the possibility of covering more wide spectral interval of the Čerenkov radiation and thus to increase the absolute intensity of the Čerenkov radiation, which is proportional to the factor

$$\left(\frac{1}{\lambda_{min}} - \frac{1}{\lambda_{max}}\right), \qquad (10)$$

where λ_{min} is the most short wavelength and λ_{max} is the most long wavelength of the spectral window of the mirror elements.

6. UNDULATOR RADIATION

The traditional undulator consists of the periodically mounted magnetic blocks, which have two permanent magnets, such as $SmCo_5$, and two working elements of the soft magnetic material (Fig.13). The magnetization of the permanent magnets is directed along the undulator axis with periodically alternated magnetization vectors. Thus the transversal periodic magnetic field is generated on the undulator axis. The accelerated electrons (Fig.14) moving along this axis produce synchrotron radiation with wavelength λ which is defined by the period length d of the transversal magnetic field of the undulator, by the energy of the electrons $E = \gamma m_0 c^2$, with m_0 - the mass of the electron, c - the velocity of the light in vacuum, γ - relativistic factor, and by the observation angle Θ:

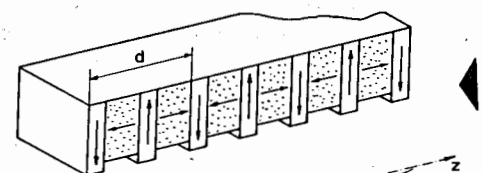

Fig.13. Traditional undulator used for production of very intense synchrotron radiation in the X-ray spectral region.

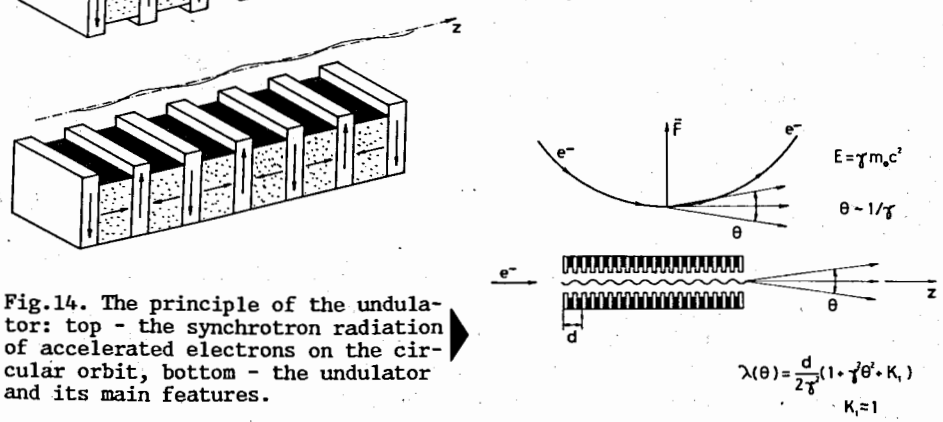

Fig.14. The principle of the undulator: top - the synchrotron radiation of accelerated electrons on the circular orbit, bottom - the undulator and its main features.

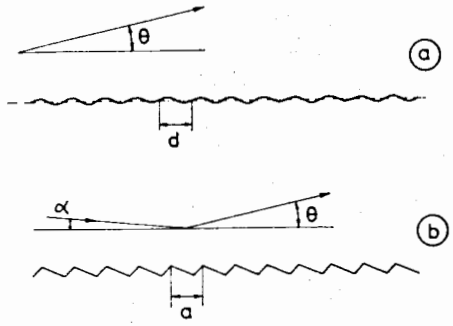

Fig.15. Virtual grating model of the undulator radiation.

$$\lambda(\Theta) = \frac{d}{2\gamma^2}(1 + \gamma^2\Theta^2 + K_1), \qquad (11)$$

where K_1 is constant which can be varied in the range $K_1 = 0 \div 4.2$ in the typical constructions of the undulator[21].

The virtual grating model of the undulator radiation[15] is indeed the phenomenological wave optical description of the undulator radiation (Fig.15). The period length of the undulator d is equal to the spacing "a" of the grooves of the virtual diffraction grating. In this model the imaginary incident angle α of the virtual radiation is equal to

$$\frac{c}{v_{eff}} = \cos\alpha \cong 1 + |\alpha|^2/2, \qquad (12)$$

where v_{eff} is the average velocity of the electrons moving along undulator axis

$$v_{eff} = c\left[1 - \frac{1}{\gamma^2}(1 + K^2/2)\right]. \qquad (13)$$

By taking into account the equation of the real diffraction grating for the first diffraction order,

$$\lambda = a(\cos\alpha - \cos\Theta), \qquad (14)$$

we get

$$\lambda = \frac{d}{2\gamma^2}(1 + \gamma^2\Theta^2 + K^2/2). \qquad (15)$$

The finite number of periods in the undulator structure N induces the additional angular divergence of the indulator radiation, $\Delta\Theta$, which for $\Theta = 0$ is equal to

$$\Delta\Theta_0 = \frac{1}{\gamma}\left(\frac{1 + K^2/2}{2N}\right)^{1/2}, \qquad (16)$$

and for $\Theta \neq 0$

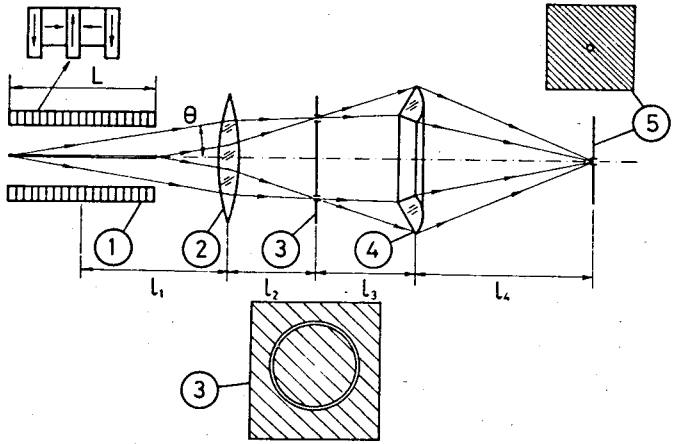

Fig.16. Inverse meso-optical system designed to focus into the point the synchrotron radiation from undulator with $\Theta \neq 0$: 1 - undulator, 2 - first inverse meso-optical objective, 3 - ring-shaped diaphragm, 4 - second inverse meso-optical objective, 5 - pinhole diaphragm.

$$\frac{\Delta\Theta}{\Theta} = \frac{1}{4N} \cdot \qquad (17)$$

The finite length L of the undulator produces some problems in focusing of the undulator radiation. Only for light rays with $\Theta = 0$ we can consider the radiation as coming from infinity. In the case of the radiation with $\Theta\gamma > 1$ we have quasimonochromatic radiation in the form of the conical wavefronts and we cannot now neglect the finite length L of the undulator.

In this angular interval we must use the inverse meso-optics. The typical meso-optical device designed for detection of side wise going undulator radiation is shown in Fig.16. The first meso-optical objective 2 transforms the conical wavefront with wave length λ_1 into a ring-shaped focus. The radiation is transmitted through the ring-shaped diaphragm 3. The quasicoherent radiation from the ring-shaped source is focused into the point on the optical axis by the second inverse meso-optical element 4. As the aperture of the first meso-optical objective 2 is greater than the aperture of the traditional lens or the diameter of the pinhole diaphragm in the case of on-axis radiation ($\Theta = 0$) the diameter of the focusing spot near the pinhole diaphragm 5 in Fig.16 will be smaller than the diameter of the traditional pinhole. The inverse meso-optical objectives 2 and 4 for radiation with wave length $\lambda \sim 10$ nm

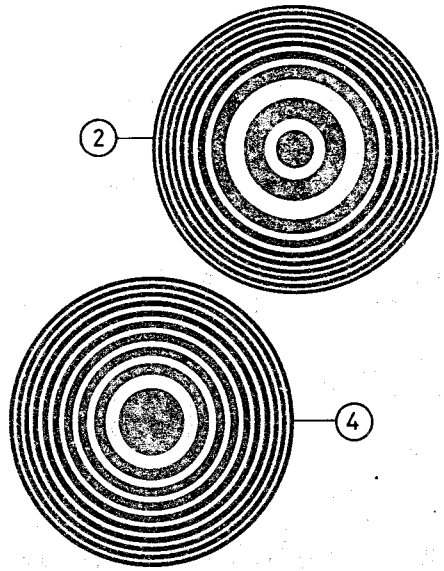

Fig.17. The binary optical relief of the inverse meso-optical diffraction elements used in the inverse meso-optical system in Fig.16.

Fig.18. Self-focusing undulator (see text).

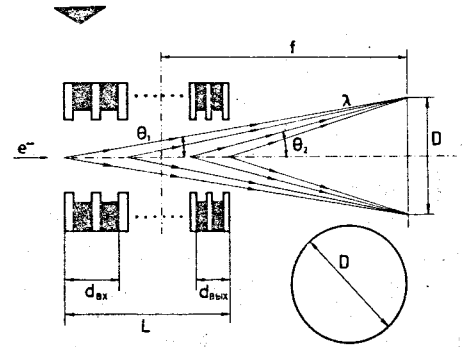

must be fabricated in the form of the diffracted elements[25] with optical profiles shown in Fig.17.

Another proposal is the self-focusing undulator (Fig.18) in which the period length d of the transversal magnetic field is a slowly varying function of z-coordinate. If f is the distance between the center of the self-focusing undulator and the ring-shaped focus, the period lengths of the undulator blocks at the input d_{in}, and at the output, d_{out}, of the undulator must be chosen in accordance with equations:

$$d_{in} = 2\gamma^2\lambda/(1 + \gamma^2\Theta_1^2 + K_1),$$

$$d_{out} = 2\gamma^2\lambda/(1 + \gamma^2\Theta_2^2 + K_1), \qquad (18)$$

where

$$\Theta_1\gamma = 1 - L/2f,$$

$$\Theta_2\gamma = 1 + L/2f. \qquad (19)$$

and with linear dependence between d_{in} and d_{out} along z-coordinate. The basic requirement of this self-focusing undulator is the wide X-ray spectrum commonly observed in the practice[24].

REFERENCES

1. Soroko L.M. - Commun. JINR, D1-82-642, Dubna, 1982.
2. Astakhov A.Yu. - Commun. JINR, P13-83-119, Dubna, 1983.
3. Koronkevitch V.P. et al. - Autometrija, Novosibirsk, 1985, 1. "Nauka", Sibir. Otd. Novosibirsk.
4. Astakhov A.Ya. et al. - Nucl. Instr. & Meth., 1989, A283, p.13.
5. McLeod J.H. - Journ. Opt. Soc. Amer., 1954, 44, p.592.
6. Mikhaltsova I.A. et al. - Optik, 1984, 67, p.267.
7. Soroko L.M. - USSR Patent No.118 39 34. Bull. No.37, 191, 1985.
8. Soroko L.M. - Commun. JINR, E13-90-592, Dubna, 1990.
9. Soroko L.M. - Commun. JINR, E13-90-593, Dubna, 1990.
10. Soroko L.M. - Commun. JINR, E13-90-594, Dubna, 1990.
11. Leseberg D. - Appl. Optics, 1987, 26, p.4385.
12. Benot M. et al. - Nucl. Instr. & Meth., 1972, 105, p.431.
13. Benot M. et al. - Nucl. Instr. & Meth., 1979, 165, p.439.
14. Meunier R. - Nucl. Instr. & Meth., 1985, A235, p.290.
15. Miyahara M. - Jap. Journ. Appl. Phys., 1986, 25, p.1672.
16. Lavender W. et al. - Rev. Sci. Instr., 1989, 60, p.1414.
17. Durnin J. - Journ. Opt. Soc. Amer., 1987, A4, p.651.
18. Durnin J. et al. - Phys. Rev. Lett., 1987, 58, p.1399.
19. Soroko L.M. - Progress in Optics, ed. E.Wolf, Elsevier, Amsterdam, 1989, 27, p.109.
20. Benot M. et al. - Nucl. Instr. & Meth., 1973, 111, p.397.
21. Peatman W. et al. - Rev. Sci. Instr., 1989, 60, p.1445.
22. Shappard C.J.R. et al. - Proc. R. Soc. London, Ser. A; 1983, 387, p.171.
23. Soroko L.M. - Commun. JINR, P13-87-468, Dubna, 1987.
24. Rarback H. et al. - Journ. X-Ray Science and Techn., 1990, 2, 274, Fig.11 for K = 1.50.
25. Kirz J. - Journ. Opt. Soc. Amer., 1974, 64, p.301.
26. Benot M., Meunier R. - Nucl. Instr. & Meth., 1980, 169, p.445.

Received by Publishing Department
on April 19, 1991.

Сороко Л.М. E13-91-175

Инверсная мезооптика и ее потенциальные применения

Описаны свойства инверсной мезооптики и ее потенциальные применения.Даны определения мезооптики и инверсной мезооптики.Показано,что в обоих случаях мы иеем дело с коническими волновыми фронтами. Рассмотрены необходимые условия, при которых можно выполнить преобразования инверсной мезооптики в рамках феноменологической модели. Дан обзор возможных применений инверсной мезооптики, в частности, в черенковском счетчике и для ондуляторного излучения. Описаны оптические свойства самофокусирующего ондулятора.

Работа выполнена в Лаборатории ядерных проблем ОИЯИ.

Сообщение Объединенного института ядерных исследований. Дубна 1991

Soroko L.M. E13-91-175

Inverse Meso-Optics and Its Potential Applications

The properties of the inverse meso-optics and its potential applications are described. The definitions of the meso-optics and the inverse meso-optics are given. It is shown that in both cases we are concerned with conical wavefronts. The necessary conditions under which the inverse meso-optical transformation can be accomplished are treated in the frame of the phenomenological model. Potential applications of the inverse meso-optics to the Čerenkov counter and to the undulator radiation are reviewed. The optical properties of the self-focusing undulator are described.

The investigation has been performed at the Laboratory of Nuclear Problems, JINR.

Communication of the Joint Institute for Nuclear Research. Dubna 1991